Journal of The Electrochemical Society, **152** (6) A1142-A1148 (2005)
0013-4651/2005/152(6)/A1142/7/$7.00 © The Electrochemical Society, Inc.

Controlled Nanoparticle Metal Phosphates (Metal = Al, Fe, Ce, and Sr) Coatings on $LiCoO_2$ Cathode Materials

Jisuk Kim,[a] Mijung Noh,[a] Jaephil Cho,[a,*,z] HyunMi Kim,[b] and Ki-Bum Kim[b]

[a]*Department of Applied Chemistry, Kumoh National Institute of Technology, Gumi, Korea*
[b]*School of Materials Science and Engineering, Seoul National University, Seoul, Korea*

Despite the fact that the same coating concentration and annealing temperature are used for MPO_4 nanoparticle coatings (M = Al, Fe, Ce, and SrH) on a $LiCoO_2$ cathode, the extent of the coating coverage is influenced by the nanoparticle size or morphology. Nanoparticles ($AlPO_4$ or $FePO_4$) with a size smaller than 20 nm led to the complete encapsulation of $LiCoO_2$, but those with sizes greater than 150 nm ($CePO_4$) or with whisker shapes ($SrHPO_4$) led to partial encapsulation. This difference affected the discharge capacity. The $LiCoO_2$ completely encapsulated with $AlPO_4$ or $FePO_4$ showed the highest discharge capacity of 230 mAh/g at 4.8 and 3 V at a rate of 0.1 C (=18 mA/g), which diminished with decreasing coating coverage in the order of Al ~ Fe < SrH < Ce < bare cathode. However, the capacity retention during cycling increased in the order of Al > Ce > SrH > Fe > bare cathode. This is consistent with the capacity retention result obtained at 90°C storage for 4 h.
 [DOI: 10.1149/1.1896526]

Manuscript submitted September 9, 2004; revised manuscript received November 17, 2004. Available electronically May 5, 2005.

In 1996, Bellcore patented an Al_2O_3, B_2O_3, and SiO_2 coating on spinel $LiMn_2O_4$ to suppress Mn dissolution from $LiMn_2O_4$ at elevated temperatures.[1] However, it was found that the irreversible capacity and capacity retention of the coated sample was inferior to the bare sample despite the lower Mn dissolution rate at 55°C storage. They reported the examples of B_2O_3-coated spinel at elevated temperature only, and there was no explanation for the decreasing capacity retention after the coating, compared with the bare cathode. Such deteriorated behavior of the coated cathode may be associated with the formation of a thick coating layer that impedes the Li diffusivity. To overcome these problems, $LiCoO_2$, which has a strong resistance to HF, was coated on the $LiMn_2O_4$ and showed improved capacity retention and lower irreversible capacity during cycling at 55°C.[2] On the other hand, $LiMn_2O_4$ was coated on $LiCoO_2$ to improve the thermal stability of the delithated Li_xCoO_2.[3] Accordingly, SnO_2, Al_2O_3, ZrO_2, and TiO_2 coatings on $LiCoO_2$ and $LiNi_{1-x}M_xO_2$ via the solgel method have been intensively investigated.[4-15] Among these coating materials, ZrO_2 coating exhibited the best capacity retention >4.5 V cycling, and high-temperature storage at 90°C. This finding was confirmed by Kim *et al.*, and among the ZrO_2, Al_2O_3, and SiO_2 coatings, the ZrO_2 coating on $LiMn_2O_4$ had to the lowest capacity fading at 55°C cycling.[14] This improvement was due to the fact that ZrO_2 behaves as an effective HF scavenger.[14] Overall, these studies revealed that the physical morphology of the coating materials significantly influenced the electrochemical properties.

Metal phosphates (M = metal ion) are of great interest for many applications, for example, as molecular sieves or size-selective catalysts, catalysts supports, or optical materials, and their application have varied depending on the pore size, particle size, and metal ions.[15-22] Dong *et al.* prepared mesoporous $AlPO_4$ by templating $AlCl_3$ and triethylphosphate with carbon spheres with a particle size of ~100 nm, which was removed by calcining at 550°C.[23] Riwtzki *et al.* reported the liquid-phase synthesis of La-, Ce-, and Te-doped $LaPO_4$ nanoparticles. In addition, they reported that higher boiling coordinating solvents such as trisethylhexyl phosphate under nitrogen for 16 h at 200°C yielded ~8 nm sized nanocrystals with an irregular 0-D.[24] Recently, the synthesis and electrochemical properties of $AlPO_4$ nanocrystals have attracted considerable interest because they have been considered to be potentially useful active coating materials for lithium intercalation compounds in Li secondary batteries.[25,26]

Recently, we found that $AlPO_4$-coated $LiCoO_2$ improved not only the 12 V overcharge stability, but also the cycling property at 4.8 V.[27,28] Using this coating method, we reported the relationship between the annealing temperature, coating concentration, and electrochemical and thermal properties. Noted that most of the coating materials were insulators. Therefore, Li conduction through this layer into the bulk material was possible via two routes. One is from the high Brunauer-Emmett-Teller (BET) surface area of the coating material, which is easily soaked with the electrolytes facilitating Li-ion pathway.[14] The other is from the formation of a Li-ion conducting solid solution (Li-M-O) between the Li in $LiCoO_2$ and the coating material during annealing.[29] A previous study on Al_2O_3-coated $LiCoO_2$ thin films reported that the surface region of the $LiCoO_2$ reacted with Al_2O_3 during charge/discharge, forming a Li-Al-O solid-solution phase on the surface. Although the coating layer has a reasonably high Li-ion conductivity, it is important to control the coating thickness so as not to increase the interfacial resistance. It was reported that the optimum coating thickness was 10-15 nm.[25]

This paper reports that effect of the nanoparticle coating (MPO_4, where M = Al, Fe, SrH, and Ce) with a different particle shape on $LiCoO_2$ cathode material. These nanoparticles showed a different morphology and particle size. Therefore, they are expected to influence the electrochemical properties after coating. Although previous coating studies focused on the electrochemical properties using a completely encapsulated cathode, this study was extended to understand the correlation between the partial encapsulation of the cathode obtained from the morphological control of the MPO_4 nanoparticles and the electrochemical properties.

Experimental

The MPO_4 nanoparticles (M = Al, Fe, SrH, and Ce) were prepared from a direct reaction between M nitrate and $(NH_4)_2HPO_4$ in distilled water M nitrate (3 g) and $(NH_4)_2HPO_4$ (1 g) were dissolved in water (25 g), and the rapid formation of white precipitates could be observed. For X-ray diffraction (XRD) and transmission electron micrscopy (TEM), the precipitates were centrifuged at 3000 rpm for 5 min, which was followed by drying and annealing at 130 and 700°C for 5 h, respectively. To coat the 10 μm sized $LiCoO_2$ cathode (100 g), cathode powders were added to the coating solution with constant stirring, which was followed by drying and annealing at 130 and 700°C for 10 and 5 h, respectively. Based upon mass spectroscopy (MS), the coating mass ratio was estimated to be 0.01 g of the coating per gram of $LiCoO_2$. The coin-type half cell consists of a cathode (94 wt %), a Li metal anode, and a separator, and the electrolyte for coin-type half cells (2016 type) was 1 M $LiPF_6$ with ethylene carbonate/diethylene carbonate/ethyl-methyl carbonate (EC/DEC/EMC) (30:30:40 vol %) (Cheil Industries, Korea). The loading level of $LiCoO_2$ studied per square cm was 35 mg. The cells for the cycling tests were tested at a charge-cutoff voltage of 4.8 V.

* Electrochemical Society Active Member.
z E-mail: jpcho@kumoh.ac.kr

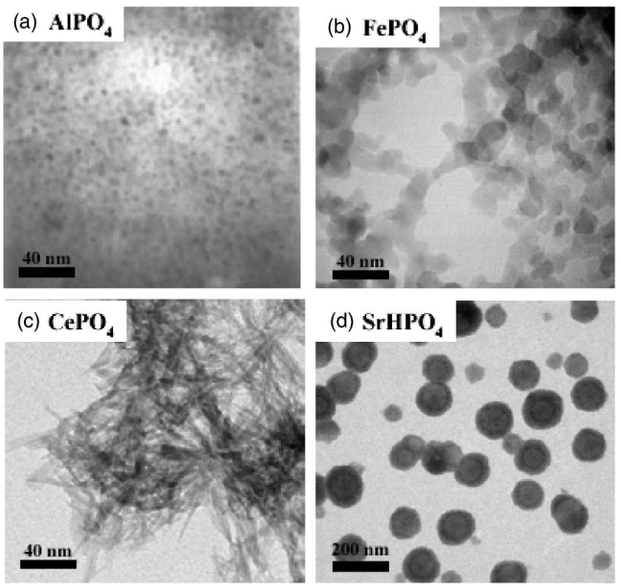

Figure 1. TEMs of MPO_4 (M = Al, Fe, Ce, and SrH) nanoparticles after drying at 130°C

The cycle-life tests were proceeded by charging and discharging at 0.1 C for the first two cycles, which was followed by a cycle at 0.2 C, a cycle at 0.5 C, and finally a cycle at 1 C (=180 mA/g) for 46 cycles. The galvanostatic intermittent titration technique (GITT) was used to estimate the Li diffusivity,[30,31] and the $Li/LiCoO_2$ test cells after finishing each 10 cycles were allowed to reach equilibrium at 4.3 V. To measure the capacity retention at 90°C, fresh cells ($Li/LiCoO_2$) were charged to 4.6 and 4.8 V and stored at 90°C for 4 h, which was then cooled to room temperature. The cells were then discharged to 3 V at a rate of 0.2 C. The Co and metal ion dissolution (M = Al, Fe, Sr, and Ce) from the bare and coated $LiCoO_2$ cathodes was measured by inductively coupled plasma-atomic emission spectroscopy (ICP-AES), and the electrolytes were obtained from the cycled cells using a centrifugal separation method. The nanoparticles and coated $LiCoO_2$ were characterized by XRD (M18XHF-SRC, MAC Science) using Cu Kα radiation in the 2θ range, 15-70°.

Results and Discussion

Figure 1 shows TEM images of the MPO_4 nanoparticles prepared in water. The particle size of the $AlPO_4$ nanoparticles was <5 nm, which was the smallest among the MPO_4 nanoparticles. On the other hand, $FePO_4$ had a larger particle size of ~20 nm while $CePO_4$ and $SrHPO_4$ were found as whisker- and spherical-type (with a particle size of 150-200 nm) nanoparticles, respectively. This indicates that the particle size and morphology was governed by the metal ion. Figure 2 shows a comparison of the XRD patterns of the precipitated nanoparticles. The XRD patterns of the $AlPO_4$ and $CePO_4$ (M = Al and Ce) particles confirmed the presence of the orthorhombic (JCPDS no. 48-652) and monoclinic phases (JCPDS no. 4-632), respectively. However, that of the $FePO_4$ shows the formation of amorphous phase. ICP-MS analysis confirmed that the stoichiometry of Fe and P was 1:1, *i.e.*, the formation of $FePO_4$. After heat-treatment at 700°C, the XRD patterns of $AlPO_4$, $FePO_4$, and $SrHPO_4$-coated $LiCoO_2$ (Fig. 3) showed only the $LiCoO_2$ phase, indicating that the coating was too thin to observe while that of the $CePO_4$-coated $LiCoO_2$ revealed the presence of crystalline CeO_2 phase. In the case of the $AlPO_4$-coated cathode, the coating thickness was estimated to be 10-15 nm.[25]

The XRD diffraction patterns of the isolated $CePO_4$ and $SrHPO_4$ particles after heat-treatment at 700°C revealed the presence of

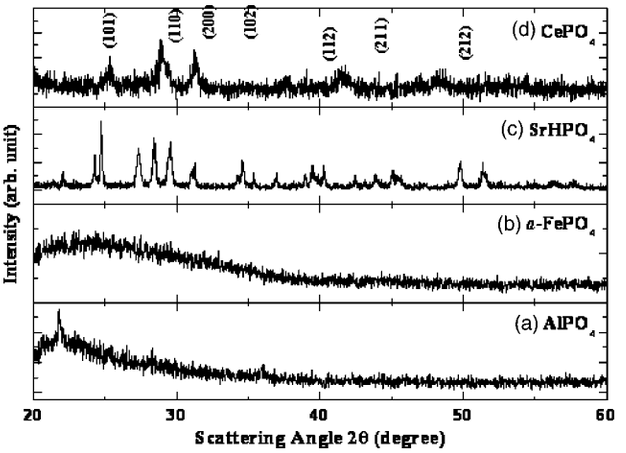

Figure 2. XRD patterns of the same nanoparticles in Fig. 1.

monoclinic $CePO_4$ (JCPDS no. 32-199), and an orthorhombic $Sr_2P_2O_7$ phase (JCPDS no. 24-1011), respectively (Fig. 4). The crystal structure of the coating layer is expected to be different from that of the isolated coating particle because MPO_4 might react with Li and even Co from the $LiCoO_2$ during annealing at 700°C, and transform into a new phase with an intrinsic stress in the nanoscale-coating layer. Hence, it is difficult to identify the coating layer phase. Despite this, the identification of the CeO_2 phase in the coated cathode suggests the existence of a completely isolated large portion of the particles from the coated cathode (this might be attributed to the partially decomposed $CePO_4$ in $LiCoO_2$ during annealing at 700°C). However, there was no secondary phase observed in the XRD pattern of the $SrHPO_4$-coated cathode, which indicates that a larger portion of the $LiCoO_2$ than $CePO_4$-coated cathode may be covered with the coating material. Electron probe micron analysis (EPMA) was performed to check the degree of encapsulation of the coated cathodes. Figure 5 shows the Co, M, and P mapping across the cross-sectioned $LiCoO_2$ particles. In the case of the $AlPO_4$ and $FePO_4$-coated $LiCoO_2$, Al and Fe elements were completely encapsulated on the particle surface in contrast to the Sr and Ce elements with the noncoating layers. On the other hand, the entire encapsulation of the cathode using the sol-gel driven Al_2O_3 and ZrO_2 coating

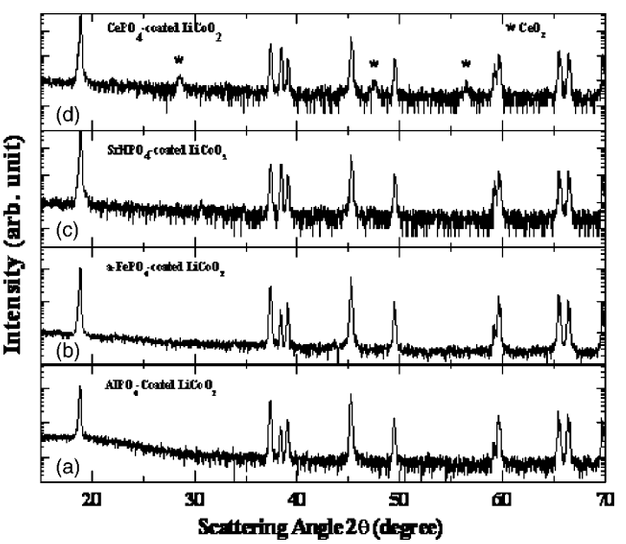

Figure 3. XRD patterns of the MPO_4-coated $LiCoO_2$ after annealing at 700°C.

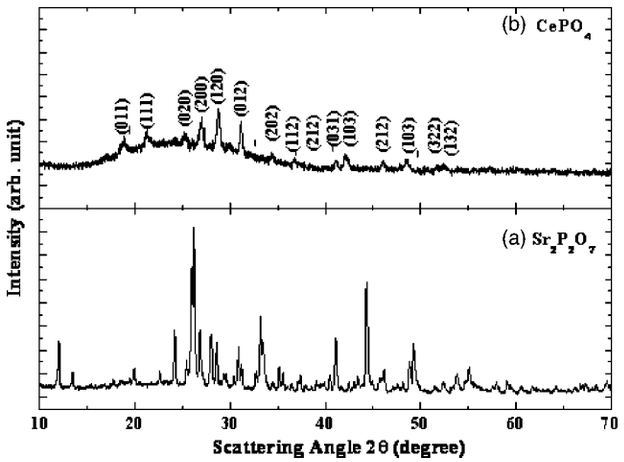

Figure 4. XRD patterns of the isolated $CePO_4$ and $SrHPO_4$ nanoparticles after annealing at 700°C. Note the phase change of $SrHPO_4$ to $Sr_2P_2O_7$ after annealing.

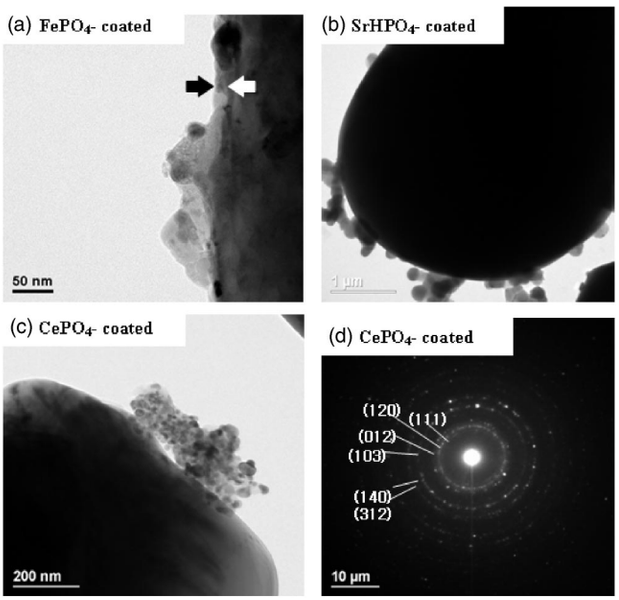

Figure 6. TEMs of (a-c) MPO_4-coated $LiCoO_2$ (M = Fe, SrH, and Ce). (d) is a SAD pattern of $CePO_4$-coated $LiCoO_2$.

was difficult to achieve. Another problem with a sol-gel coating is that it cannot control the coating thickness. For example, the TEM images reported by Thackeray's group and Dahn's group showed such evidence.[14,32-34] However, the nanoparticle coating exhibited very good coating coverage and coating thickness could be controlled by the nanoparticle size.

The EPMA result is well consistent with the TEM images of the MPO_4-coated $LiCoO_2$ (Fig. 6), and the $FePO_4$-coated $LiCoO_2$ shows a completely covered coating layer with a thickness of ~25 -50 nm, which is thicker than the $AlPO_4$-coated $LiCoO_2$(~15 -20 nm).[35] This is due to the larger $FePO_4$ particles than $AlPO_4$, even though the same coating concentration (1 wt %) was used. In the case of $CePO_4$ and $SrHPO_4$, only a portion of the $LiCoO_2$ was

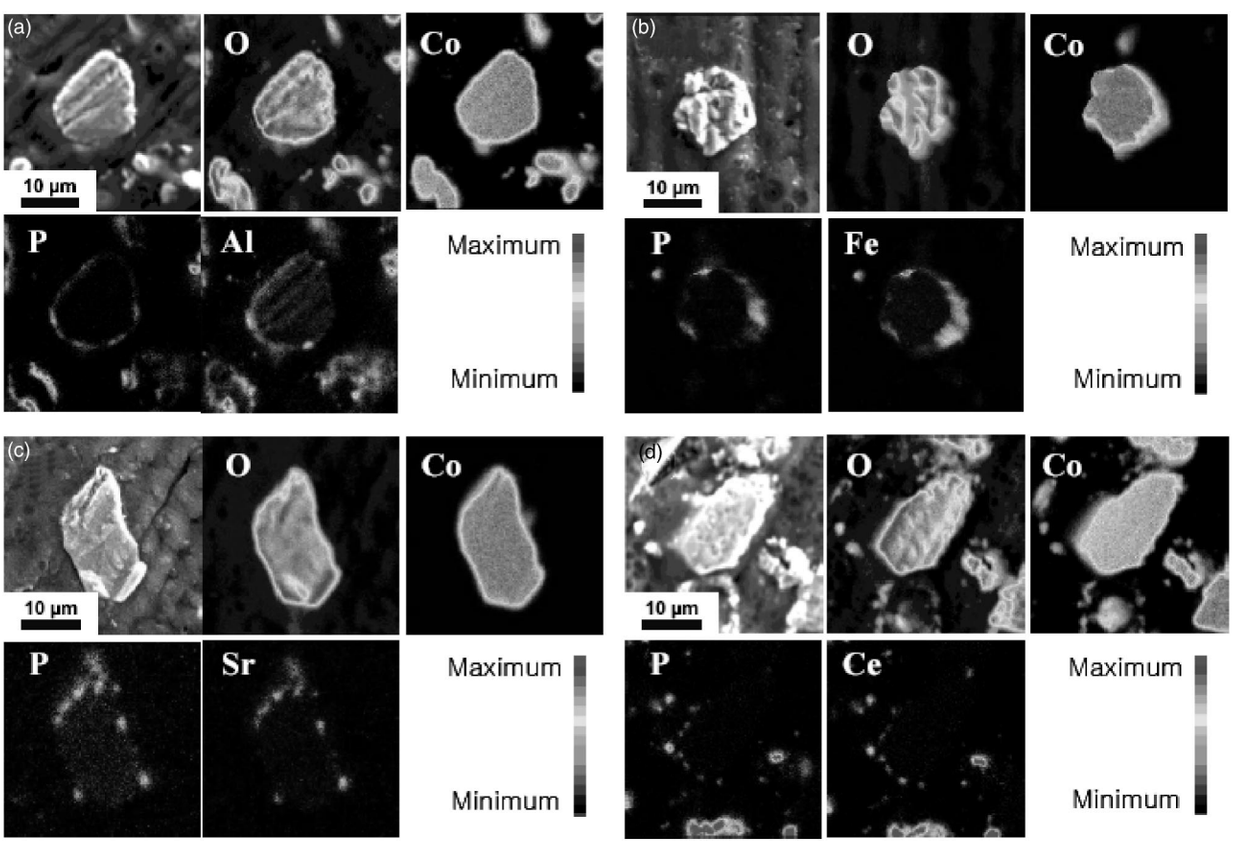

Figure 5. EPMA of cross section MPO_4-coated $LiCoO_2$ cathodes.

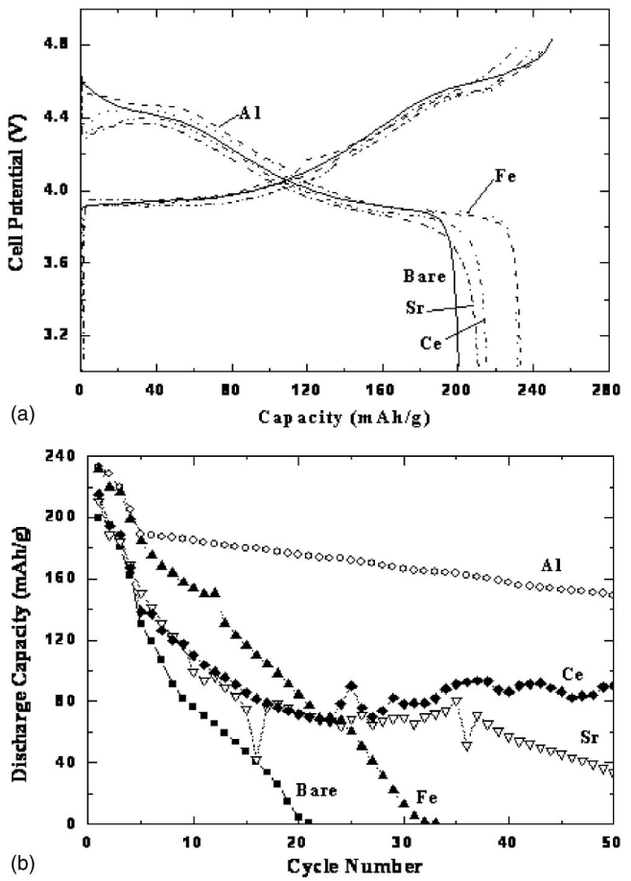

Figure 7. Plots of (a) discharge profiles of MPO_4-coated $LiCoO_2$ in coin-type half cell at 0.1 C between 4.8 and 3 V and (b) cycling number *vs.* discharge capacity.

covered with the particles. However, it is interesting to note that the original whisker type particle morphology of the $CePO_4$ was completely changed into an aggregation of ~30-40 nm sized particles. Selected area diffraction (SAD) of the coating particle of the $CePO_4$-coated $LiCoO_2$ confirmed the presence of a $CePO_4$ phase that did not transform into the other phases from the interfacial reaction. This indicates that $CePO_4$ is inert. However, the crystal structure of the $SrHPO_4$-coated cathode showed mixed phases with several different structures. As mentioned above, the observation of a secondary CeO_2 phase in the XRD pattern of the $CePO_4$-coated cathode may result from the isolated particles. Therefore, a portion of the completely isolated $Sr_2P_2O_7$ and CeO_2 particles from the coated $LiCoO_2$ should exist in the $LiCoO_2$ particles.

Such partial encapsulation is related to the BET surface area of the nanoparticles, and the values for M = Al, Fe, SrH, and Ce corresponds to 25, 16, 8, and 3 m^2/g, respectively. Because the nanoparticles adsorbed on the cathode are only possible through the physical bonding during the drying process at 130°C, those with a higher BET surface area should have a larger wetting area on the $LiCoO_2$. Hence, there is no doubt that the $AlPO_4$ and $FePO_4$ particles can easily wet the $LiCoO_2$, compared with $SrHPO_4$ and $CePO_4$. On the other hand, the physical bonding was hardened via a chemical reaction between the Li in $LiCoO_2$ during annealing at 700°C. Figure 7 shows voltage profiles of the MPO_4-coated $LiCoO_2$ between 3 and 4.8 V at the rate of 0.1 C. The coating level was estimated as ~1 wt %. Therefore, the capacity contribution was believed to be negligible. To understand Li conduction mechanism, Al_2O_3-coated $LiCoO_2$ using sputtering method was tested.[20] This result showed that the independence of the Al_2O_3 thickness on the electrochemical properties in the thin-film geometry indicated that the oxide coating layer acted as a solid electrolyte with a low electronic conductivity and a reasonably high Li-ion conductivity. In the case of the MPO_4-coated cathodes, the formation of a Li-M-P-O solid-solution coating layer was expected during the cycles although the $AlPO_4$ and $Sr_2P_2O_7$ phases are electrochemically inactive, and $CePO_4$ and $FePO_4$ are electrochemically active. As the coating thickness increases, the reaction of Li might become slower and less efficient due to the limited electronic conduction among the particles. Note that the MPO_4-coated $LiCoO_2$ (M = Ce, SrH, and Fe) exhibits a large drop in the IR drop upon a 0.1 C rate discharge. This is related to the coating thickness because a similar behavior was observed in the $AlPO_4$-coated cathodes with a coating thickness with >20 nm.[25] Hence, the $FePO_4$ with a coating thickness of ~20-50 nm can be influenced by the reduction in the IR drop. However, the $LiCoO_2$ that is partially covered with $CePO_4$ and $SrHPO_4$ particles was observed to have a larger IR drop than the others. This suggests that the isolated nonconducting $Sr_2P_2O_7$ and CeO_2 particles play a key role reducing the initial potential. In addition, the possibility that partially encapsulating the coating layers with $SrHPO_4$ and $CePO_4$-coated cathodes contributes to such an IR drop cannot be ruled out.

The discharge capacities of the completely encapsulated $FePO_4$ and $AlPO_4$-coated $LiCoO_2$ shows the highest discharge capacity, 230 mAh/g, and the $LiCoO_2$ cathodes with partially covered with $SrHPO_4$ and $CePO_4$ shows ~210 mAh/g. For example, the amount of Co dissolution after the first cycling increased in the order of bare (1053 ppm) > SrH ~ Ce (230 and 210 ppm) > Fe ~ Al (50 and 40 ppm, respectively). However, the bare sample showed the smallest capacity of 190 mAh/g. This clearly shows that the degree of coverage affects the discharge capacity, and a complete coverage was reported reduce the Co dissolution rate or any other side reactions between the particle surface and the electrolytes at the higher cutoff voltages.[26] According to Aurbach *et al.*, upon cycling or storage at the elevated temperatures, capacity loss of the $LiCoO_2$ electrodes cycled to 4.2 V was caused by the formation of surface films that covered the particles, which might electronically isolate them from each other and from the current collector.[35] Similarly, such an electronically resistive surface film may form even faster and cause more rapid capacity loss when the electrode is cycled above 4.5 V than when it is cycled to 4.2 V.[24] In addition, Co dissolution was accompanied by the loss of Li from the Li_xCoO_2 structure, resulting in a loss of Li insertion/extraction sites.[36] This can eventually hinder the Li insertion/desertion sites and cause capacity fading. However, the amount of Co dissolution after 50 cycles reveals that that the $AlPO_4$-coated cathode is similar to that of the $FePO_4$-coated cathode, which is in contrast to the $SrHPO_4$ and $CePO_4$-coated cathodes (Fig. 8). Despite this, it is interesting to note that the $FePO_4$-coated cathodes continue to reduce to 0 mAh/g after 25 cycles while capacity fading of the $CePO_4$ and $SrHPO_4$-$LiCoO_2$ was slow, showing 90 and 38 mAh/g, respectively, after 50 cycles (Fig. 7). Moreover, this suggests that such a rapid capacity fading of the $FePO_4$-coated cathode did not originate from Co dissolution but from a decrease in Li mobility as a result of the coating layer.

The Li diffusivities of the bare and coated cathodes were estimated after 10, 20, 30, 40, and 50 cycles using GITT at 4.3 V. As shown in Fig. 8, the Li diffusivity of the $FePO_4$-coated cathode rapidly decreases with cycling in contrast to the $AlPO_4$-coated cathode. On the other hand, a trend of Co dissolution well agrees with that of the Li diffusivity in the bare, $SrHPO_4$ and $CePO_4$-coated cathodes. Accordingly, the rapid capacity fading of the $FePO_4$-coated cathode is due to the decreased Li diffusivity with cycling, but that of the $SrHPO_4$ and $CePO_4$-coated cathodes correlated with the Co dissolution. However, it is expected that the higher capacity retention of the $SrHPO_4$ and $CePO_4$-coated cathodes than the bare cathode is due to the fact that a partially formed coating layer suppresses Co dissolution. These results clearly show a much higher Li diffusivity of the coated cathodes along with excellent

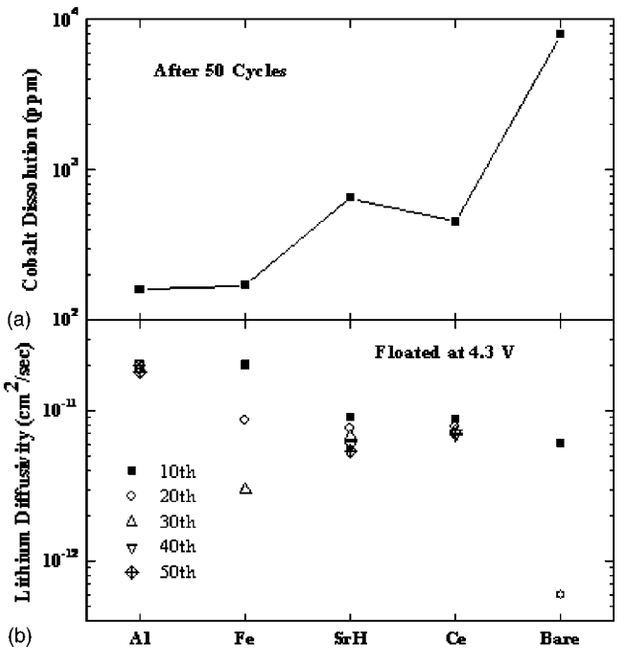

Figure 8. Plots of (a) Co dissolution of bare and MPO_4-coated $LiCoO_2$ and (b) lithium diffusivity of the bare and MPO_4-coated cathodes after 10, 20, 30, 40, and 50 cycles.

capacity retention during cycling than the bare cathode, indicating that the formation of an electrically resistive film on the cathode was suppressed. Recently, Chen and Dahn reported that the cycle-life performance of $LiCoO_2$ was improved by a simple heat-treatment, due to the elimination of surface contamination on the cathode, for example, moisture, organic species, etc.[33,34] However, our study found that the thermal history of the bare powders did not improve the electrochemical properties. The powder size used by Chen and Dahn is smaller than the conventional ~10 μm sized powders.[9,25,26]

In relation to Co dissolution, Fig. 9 shows the lattice constants *a* and *c* and the *c*/*a* ratio of the coated cathodes (at the discharged state of 3 V) after cycles, which changes less than those of the bare cathode. During cycling, the surface of the bare cathode was damaged due to Co dissolution, and Li intercalation/deintercalation through this structurally damaged region was difficult. In contrast, the coating layer suppresses Co dissolution. Therefore, the surface region of the coated $LiCoO_2$ cathodes fully encapsulated with $AlPO_4$ and $FePO_4$ may be less damaged, compared with that of the cathodes that were partially encapsulated with $SrHPO_4$ and $CePO_4$. Furthermore, to investigate the structural changes after cycling, five peaks ((0 0 3), (1 0 1), (1 0 4), (0 1 5), and (0 1 8)) were fitted from the patterns.

Peak-broadening may be associated with either microstructural defects or a non-uniform distribution of local strain.[36,37] The peak widths Δk (full width at half maximum, fwhm) were fitted for each peak with a scattering vector $k = (4\pi/\lambda)\sin\theta$ using a double-peak Lorentzian function for $K\alpha_1$ and $K\alpha_2$. The effective grain size estimated from the intercept at $k = 0$ does not show any systematic changes due to the large error in the fitting process. Figure 10 shows the local strain in the cathodes before and after cycling with a charge cutoff voltage of 4.8 V, as a function of the coating material. The inset is a representative Δk *vs.* k plot in the $SrHPO_4$-coated sample measured at 3 V after 50 cycles. The local strain in the cathodes can be estimated from the slope of the Δk *vs.* k plot after subtracting the resolution function ($\Delta k_{res} = 0.076\text{-}0.00033k(\text{nm}^{-1})$). The local strain in the bare sample after 50 cycles increased approximately by a factor of four in comparison with the $AlPO_4$ and $FePO_4$-coated cathodes. Note that the change in the local strain is quite consistent

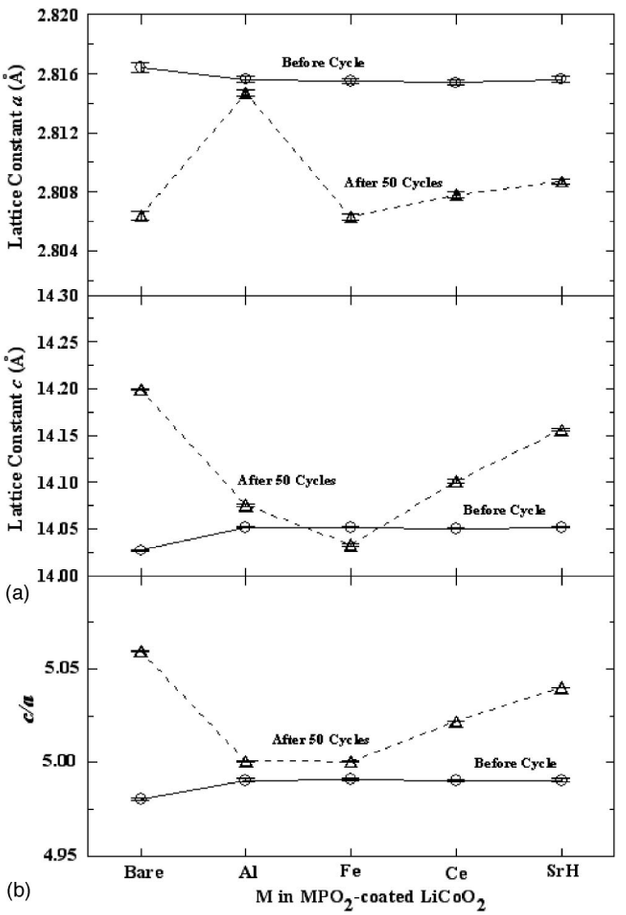

Figure 9. Plots of (a) the lattice constants *a* and *c*, and (b) *c*/*a* ratio (at the discharged state) in the bare and MPO_4-coated $LiCoO_2$ cathodes (M = Al, Fe, Ce, and SrH), after 50 cycles with 4.8 V.

with that of Co dissolution, increasing in the order of Al ~ Fe < Ce < SrH. The analysis of local strain in Fig. 10 clearly demon-

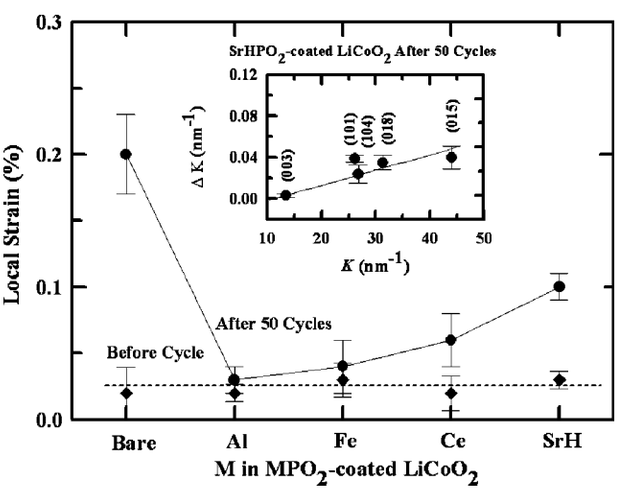

Figure 10. The local strain in the cathodes before and after cycling with a charge cutoff voltage of 4.8 V, as a function of the coating material. The inset is a representative Δk *vs.* k plot in the $SrHPO_4$-coated sample measured at 3 V after 50 cycles.

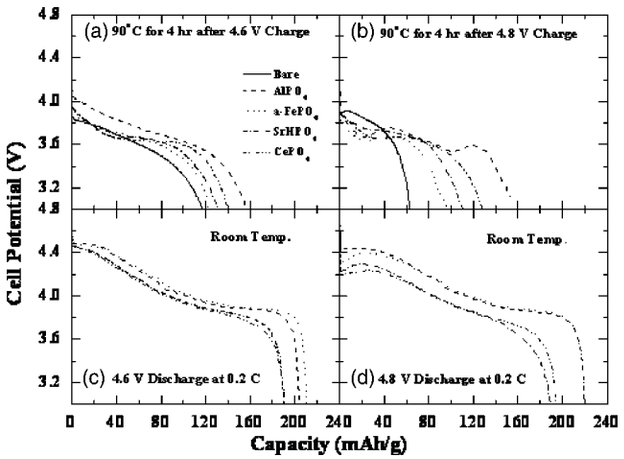

Figure 11. Plots of the discharge capacities of the bare and MPO_4-coated $LiCoO_2$ at (a-b) 90°C for 4 h storage, and (c-d) room temperature. The discharge rate was 0.2 C.

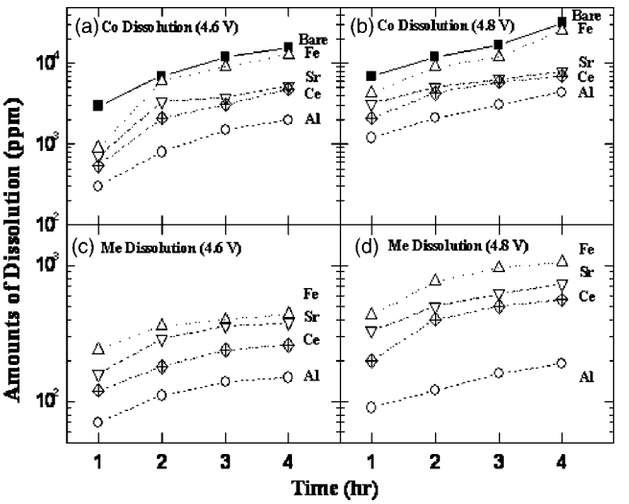

Figure 12. Plots of Co and metal ions (Me) in the MPO_4-coated cathodes at 90°C as a function of the storage time (Me = Al, Fe, Ce, and Sr).

strates that the MPO_4-nanoparticle coating effectively suppresses the structural degradation caused by Co dissolution.

Figure 11 shows the discharge capacities of the bare and coated cathodes at 0.2 C at room temperature and after 90°C storage at 4 h at 4.6 and 4.8 V charge cutoffs. The trend of the discharge capacity is quite similar to the capacity retention at room temperature, and decreased in the order of Al < Ce < Sr < Fe < bare. In addition, severe reductions in capacity were observed at 90°C, compared with those at room temperature. It was observed that the Li metal was partially damaged and covered with some decomposed electrolyte products at 90°C. Hence, the decrease in capacity may be partly due to this effect. However, there is a good correlation between the 90°C storage data. The $AlPO_4$-coated cathode shows no capacity decay at both 4.6 and 4.8 V, which is in contrast to the other coated cathodes. For example, the capacity of the $CePO_4$, $SrHPO_4$, and $FePO_4$-coated cathodes decreased from 140, 130, and 123 mAh/g to 128, 110, and 98 mAh/g, respectively, when the charge cutoff voltage increased from 4.6 to 4.8 V. In particular, the largest capacity drop of the $FePO_4$-coated cathodes was surprising. Even though this cathode shows comparable capacity to the $AlPO_4$-coated cathode at room temperature, the capacity drop at 90°C may be related to other factors. Previous studies revealed that Co dissolution is concomitant with the dissolution of Li into the electrolyte, leading to the destruction of the Li_xCoO_2 structure.[36] Once a uniform coating layer is present, Co dissolution should be minimized, and its value is expected to be similar to be that of the $AlPO_4$-coated $LiCoO_2$. However, these results showed that the $CePO_4$ and $SrHPO_4$-coated cathodes had better capacity retention than $FePO_4$.

To investigate the origin, the amounts of Co and Metal ion dissolution (Me = Al, Fe, Ce, and Sr) from the MPO_4-coated $LiCoO_2$ were measured at 4.6 and 4.8 V after storage at 90°C for 1, 2, 3, and 4 h, as shown in Fig. 12. Fe dissolution showed the highest value, and M dissolution decreased in the order of Ce < Sr < Al, which is well consistent with that of capacity retention after 90°C storage. In addition, Co dissolution continues to increase with increasing storage time in all the coated cathodes, but $AlPO_4$-coated cathode shows the lowest amount Co dissolution. For example, the $FePO_4$-coated $LiCoO_2$ shows a six times larger amount of dissolution than $AlPO_4$-coated cathode. This suggests that, capacity retention at 90°C is governed by M dissolution in contrast to that at room temperature. It is interesting to note that the $SrHPO_4$ and $CePO_4$ showed less Co and M dissolution than $FePO_4$. This is due to the lower Sr and Ce dissolution rate than Fe. This result indicates that Sr and Ce ions are relatively stable at higher temperatures than Fe ions. When the Co dissolution time was extended to 24 h, there was clearer evidence that the metal phosphate coatings minimized the Co dissolution except for the $FePO_4$-coated cathode. The amounts of co dissolution from the bare, $AlPO_4$-coated, $CePO_4$-coated, $SrHPO_4$-coated, and $FePO_4$-coated cathodes increased from 32,000, 4,400, 7,000, 7,900, and 26,000 ppm, respectively, to 98,700, 5,000, 9,500, 10,000, and 65,000 ppm, respectively.

Conclusions

The coating coverage on the $LiCoO_2$ cathode strongly depended on the MPO_4 nanoparticle size and morphology even though the same coating concentration was used. Hence, $FePO_4$ and $AlPO_4$ with particle sizes smaller than 20 nm exhibited complete encapsulation compared with $SrHPO_4$ and $CePO_4$, which had isolated coating layers. More surprisingly, the $SrHPO_4$ and $CePO_4$-coated cathodes showed better capacity retention than $FePO_4$ at 90°C storage. This was attributed to the continuous Fe metal ion dissolution at 90°C at the highly delithiated Li_xCoO_2, and a higher amount of Fe ions was dissolved into the electrolytes than the $SrHPO_4$ and $CePO_4$-coated cathodes. Therefore, the elevated temperature performance of the coated cell was influenced by the metal ion in the MPO_4 in contrast to that at room temperature. In conclusion, an $AlPO_4$ coating with a particle size and coating thickness <3 nm and <10-15 nm, respectively, showed the best electrochemical performance.

Acknowledgment

The authors thank Joon-Gon Lee, Tae-Gon Kim, and Professor Byungwoo Park for helpful discussions and XRD/TEM/EPMA analysis for the MPO_4-coated cathodes. This work was supported by the Basic Research Program (R01-2004–000–10173–0) of KOSEF. This work was also partially supported by KOSEF through the Research Center for Energy Conversion and Storage at Seoul National University.

The Kumoh National Institute of Technology assisted in meeting the publication costs of this article.

References

1. G. G. Amatucci and J. -M. Tarascon, U.S. Pat. 5705291 (1996).
2. J. Cho and G. Kim, *Electrochem. Solid-State Lett.*, **2**, 253 (1999).
3. J. Cho, C. S. Kim, and S. I. Yoo, *Electrochem. Solid-State Lett.*, **3**, 362 (2000).
4. J. Cho, G. Kim, H. S. Lim, C. S. Kim, and S. I. Yoo, *Electrochem. Solid-State Lett.*, **2**, 607 (1999).
5. J. Cho, Y. J. Kim, and B. Park, *Chem. Mater.*, **12**, 3788 (2000).
6. J. Cho, Y. J. Kim, T. -J. Kim, and B. Park, *Angew. Chem., Int. Ed.*, **40**, 3367 (2001).
7. (a) J. Cho, Y. J. Kim, T. -J. Kim, B. Park, *Chem. Mater.*, **13**, 10 (2001); (b) J. Cho,

Y. J. Kim, T. -J. Kim, and B. Park, *Chem. Commun. (Cambridge)*, **2001**, 1074.
8. J. Cho, *Chem. Mater.*, **13**, 4537 (2001).
9. H. -J. Kweon and D. G. Park, *Electrochem. Solid-State Lett.*, **3**, 128 (2000).
10. B. V. R. Chowdrai, G. V. S. Rao, and S. Y. Chow, *J. Solid State Electrochem.*, **6**, 565 (2002).
11. A. M. Kannan, L. Rabenberg, and A. Manthiram, *Electrochem. Solid-State Lett.*, **5**, A213 (2002).
12. Z. R. Zhang, H. S. Liu, Z. L. Gong, and Y. Yang, *J. Electrochem. Soc.*, **151**, A599 (2004).
13. H. Omanda, T. Brousse, C. Marhic, and D. M. Schleich, *J. Electrochem. Soc.*, **151**, A922 (2004).
14. J. -S. Kim, C. S. Johnson, J. T. Vaughey, S. A. Hackney, K. A. Walz, W. A. Zeltner, M. Z. Anderson, and M. M. Thackeray, *J. Electrochem. Soc.*, In press.
15. M. Pasquali, S. Passerini, and G. Pistoia, in *Science and Technology of Lithium Batteries*, G.-H. Nazari and G. Pistoia, Editors, Kluwer Academic Publishers, Norwell, MA (2003), and references therein.
16. J. Jimenez-Jimenez, P. Maireles-Torres, P. Olivera-Pastor, E. Rodriguez-Castellon, A. Jimenez-Lopez, D. J. Jones, and J. Roziere, *Adv. Mater. (Weinheim, Ger.)*, **10**, 812 (1998).
17. M. Tiemann and M. Froba, *Chem. Mater.*, **13**, 3211 (2001).
18. C. N. R. Rao, S. Natarajan, A. Choudhury, S. Neeraj, and A. A. Ayi, *Acc. Chem. Res.*, **34**, 80 (2001).
19. C. Serre, A. Auroux, M. Hervieu, and M. Ferey, *Angew. Chem., Int. Ed.*, **41**, 1594 (2002).
20. A. Bibby and L. Mercier, *Chem. Mater.*, **14**, 1594 (2002).
21. D. Zhao, A. Luan, and L. Kevan, *Chem. Commun. (Cambridge)*, **1997**, 1009.
22. U. Ciesla, S. Schacht, G. D. Stucky, K. K. Unger, and F. Schuth, *Angew. Chem., Int. Ed. Engl.*, **25**, 541 (1996).
23. A. Dong, N. Ren, Y. Tang, Y. Wang, Y. Zhang, W. Hua, and Z. Gao, *J. Am. Chem. Soc.*, **125**, 4976 (2003).
24. (a) K. Riowotzki, H. Meyssamy, A. Kornowski, and M. Hasse, *J. Phys. Chem. B*, **104**, 2824 (2000); (b) T. Nutz and M. Hasse, *J. Phys. Chem. B*, **104**, 8430 (2000); (c) S. Heer, O. Lehmann, M. Hasse, H. -U. Gudel, *Angew. Chem., Int. Ed.*, **42**, 3179 (2003).
25. J. Cho, Y. W. Kim, B. Kim, and B. Park, *Angew. Chem., Int. Ed.*, **42**, 16181 (2003).
26. J. Cho, J. -G. Lee, B. Kim, and B. Park, *Chem. Mater.*, **15**, 3190 (2003).
27. J. Cho, *Electrochem. Commun.*, **5**, 146 (2003).
28. J. -G. Lee, B. Kim, J. Cho, Y. -W. Kim, and B. Park, *J. Electrochem. Soc.*, **151**, A805 (2004).
29. Y. J. Kim, H. Kim, B. Kim, D. Ahn, J. -G. Lee, T. -J. Kim, D. Son, J. Cho, Y. -W. Kim, and B. Park, *Chem. Mater.*, **15**, 1505 (2003).
30. Y. -M. Choi, S. -I. Pyun, J. -S. Bae, and S. -I. Moon, *J. Power Sources*, **56**, 25 (1995).
31. P. Birke, W. F. Chu, W. Weppner, *Solid State Ionics*, **93**, 1 (1997).
32. Z. Chen and J. R. Dahn, *Electrochim. Acta*, **49**, 1079 (2004).
33. Z. Chen and J. R. Dahn, *Electrochem. Solid-State Lett.*, **7**, A11 (2004).
34. Z. Chen and J. R. Dahn, *Electrochim. Acta*, **49**, 1079 (2004).
35. D. Aurbach, B. Markovsky, A. Rodkin, E. Levi, Y. S. Cohen, O. Palchik, H. -J. Kim, and M. Schmidt, *Electrochim. Acta*, **47**, 4291 (2002).
36. G. G. Amatucci, J. -M. Tarascon, and L. C. Klein, *Solid State Ionics*, **83**, 167 (1996).
37. Y. Kim, J. Oh, T.-G. Kim, and B. Park, *Appl. Phys. Lett.*, **78**, 2363 (2001).